



AFRL-RZ-WP-TP-2010-2109

**A MIXING PLANE MODEL INVESTIGATION OF
SEPARATION AND TRANSITIONAL FLOW AT LOW
REYNOLDS NUMBERS IN A MULTISTAGE LOW
PRESSURE TURBINE (POSTPRINT)**

Darius D. Sanders and Walter F. O'Brien

Virginia Tech

Rolf Sondergaard, Marc D. Polanka, and Douglas C. Rabe

Turbine Branch

Turbine Engine Division

JANUARY 2009

Approved for public release; distribution unlimited.

See additional restrictions described on inside pages

STINFO COPY

**AIR FORCE RESEARCH LABORATORY
PROPULSION DIRECTORATE
WRIGHT-PATTERSON AIR FORCE BASE, OH 45433-7251
AIR FORCE MATERIEL COMMAND
UNITED STATES AIR FORCE**

REPORT DOCUMENTATION PAGE

Form Approved
OMB No. 0704-0188

The public reporting burden for this collection of information is estimated to average 1 hour per response, including the time for reviewing instructions, searching existing data sources, gathering and maintaining the data needed, and completing and reviewing the collection of information. Send comments regarding this burden estimate or any other aspect of this collection of information, including suggestions for reducing this burden, to Department of Defense, Washington Headquarters Services, Directorate for Information Operations and Reports (0704-0188), 1215 Jefferson Davis Highway, Suite 1204, Arlington, VA 22202-4302. Respondents should be aware that notwithstanding any other provision of law, no person shall be subject to any penalty for failing to comply with a collection of information if it does not display a currently valid OMB control number. **PLEASE DO NOT RETURN YOUR FORM TO THE ABOVE ADDRESS.**

1. REPORT DATE (DD-MM-YY) January 2009			2. REPORT TYPE Conference Paper Postprint		3. DATES COVERED (From - To) 01 January 2009 – 31 January 2009	
4. TITLE AND SUBTITLE A MIXING PLANE MODEL INVESTIGATION OF SEPARATION AND TRANSITIONAL FLOW AT LOW REYNOLDS NUMBERS IN A MULTISTAGE LOW PRESSURE TURBINE (POSTPRINT)					5a. CONTRACT NUMBER In-house	
					5b. GRANT NUMBER	
					5c. PROGRAM ELEMENT NUMBER 61102F	
6. AUTHOR(S) Darius D. Sanders and Walter F. O'Brien (Virginia Tech) Rolf Sondergaard, Marc D. Polanka, and Douglas C. Rabe (AFRL/RZTT)					5d. PROJECT NUMBER 2307	
					5e. TASK NUMBER NP	
					5f. WORK UNIT NUMBER 2307NP02	
7. PERFORMING ORGANIZATION NAME(S) AND ADDRESS(ES) Virginia Tech Mechanical Engineering Department Blacksburg, VA 24061				8. PERFORMING ORGANIZATION REPORT NUMBER AFRL-RZ-WP-TP-2010-2109		
9. SPONSORING/MONITORING AGENCY NAME(S) AND ADDRESS(ES) Air Force Research Laboratory Propulsion Directorate Wright-Patterson Air Force Base, OH 45433-7251 Air Force Materiel Command United States Air Force				10. SPONSORING/MONITORING AGENCY ACRONYM(S) AFRL/RZTT		
				11. SPONSORING/MONITORING AGENCY REPORT NUMBER(S) AFRL-RZ-WP-TP-2010-2109		
12. DISTRIBUTION/AVAILABILITY STATEMENT Approved for public release; distribution unlimited.						
13. SUPPLEMENTARY NOTES Conference paper published in the Proceedings of the AIAA Aerospace Science Meeting, January 2009, held in Orlando, FL. PA Case Number: 88ABW-2009-1536; Clearance Date: 15 Apr 2009. Paper contains color. The U.S. Government is joint author of the work and has the right to use, modify, reproduce, release, perform, display, or disclose the work.						
14. ABSTRACT Steady flow CFD simulations of multistage LPT flow were completed at nominal and high altitude conditions with the conventional Spalart-Allmaras turbulence model. This model was used in combination with a mixing plane model for the simulation of flow through domains with one or more regions in relative rotational motion. Flow visualizations were completed using surface flow and streamline calculations to help identify vortical structures present within the flowfield. Also, the total pressure loss coefficient was calculated for each blade row. Qualitative comparisons indicate that the simulated high altitude condition had an increase in the amount of separated flow present within the flowfield compared to the nominal altitude condition.						
15. SUBJECT TERMS low pressure turbine (LPT), separation, turbulence and transition models, computational modeling.						
16. SECURITY CLASSIFICATION OF:			17. LIMITATION OF ABSTRACT: SAR	18. NUMBER OF PAGES 22	19a. NAME OF RESPONSIBLE PERSON (Monitor) Rolf Sondergaard 19b. TELEPHONE NUMBER (Include Area Code) N/A	
a. REPORT Unclassified	b. ABSTRACT Unclassified	c. THIS PAGE Unclassified				

A Mixing Plane Model Investigation of Separation and Transitional Flow at Low Reynolds Numbers in a Multistage Low Pressure Turbine

Darius D. Sanders¹ and Walter F. O'Brien²

Mechanical Engineering Department, Virginia Tech, Blacksburg, VA, 24061 USA

Rolf Sondergaard³, Marc D. Polanka⁴, and Douglas C. Rabe⁵

Air Force Research Lab, Propulsion Directorate, Wright-Patterson AFB, OH, USA

Flow separation with increased losses is known to occur when low pressure turbine (LPT) blades are operated at high altitudes with a reduced inlet Reynolds number. Under these conditions, boundary layer separation is more likely to be present within the flowfield of the LPT stages due to thickening of the boundary layers and an increase in the portion of the airfoil experiencing laminar flow. More accurate CFD predictions are needed in order to improve design methods and performance prediction for LPT stages operating at low Reynolds numbers. Steady flow CFD simulations of multistage LPT flow were completed at nominal and high altitude conditions with the conventional Spalart-Allmaras turbulence model. This model was used in combination with a mixing plane model for the simulation of flow through domains with one or more regions in relative rotational motion. Flow visualizations were completed using surface flow and streamline calculations to help identify vortical structures present within the flowfield. Also, the total pressure loss coefficient was calculated for each blade row. Qualitative comparisons indicate that the simulated high altitude condition had an increase in the amount of separated flow present within the flowfield compared to the nominal altitude condition. This can be attributed to the reduction in the inlet Reynolds number. Initial investigations with a recently-developed three-equation eddy-viscosity type turbulent transitional flow model are also reported. Comparisons of flow predictions for the 1st turbine stage with the two models revealed that large vortices predicted with the Spalart-Allmaras model were not present, and the wake loss coefficient was significantly lower with the three-equation turbulence model. Based on these and previous results, the CFD with the three-equation model is considered to have potential to provide improved prediction of separation and transitional flow in low Reynolds number turbine applications.

Nomenclature

d	=	wall distance
D	=	kinetic energy near-wall dissipation
k	=	kinetic energy
l_m	=	average turbulent length scale
P	=	pressure; production term
r	=	radius
R	=	bypass transition production term
R_{NAT}	=	natural transition production term
Re	=	Reynolds number based on axial chord

¹ Graduate Student, Virginia Tech, Mechanical Engineering, AIAA Student Member

² J. Bernard Jones Professor, Virginia Tech, Mechanical Engineering; AIAA Associate Fellow

³ Research Engineer, AFRL/RZTT, 1950 Fifth St. Bldg 18 WPAFB, OH 45433, AIAA Associate Fellow

⁴ Research Engineer, AFRL/RZTE, 1950 Fifth St. Bldg 18 WPAFB, OH 45433, AIAA Associate Fellow

⁵ Turbine Engine Research Center Director, AFRL/RZTE, 1950 Fifth St. Bldg 18 WPAFB, OH 45433, AIAA Associate Fellow

t	=	time
LPT	=	low pressure turbine
TPLC	=	total pressure loss coefficient
Tu	=	freestream turbulent intensity
u	=	velocity magnitude
u'	=	streamwise fluctuation
x	=	directional component
y^+	=	nondimensional wall distance
α_T	=	turbulent diffusivity
δ_{ij}	=	Kronecker delta
λ_{eff}	=	effective length scale
λ_T	=	integral turbulent length scale
μ	=	molecular viscosity
ν	=	kinematic viscosity
$\tilde{\nu}$	=	modified kinematic viscosity
ρ	=	density
ω	=	specific dissipation rate

Subscripts

0	=	total
i,j	=	indices
in	=	inlet
L	=	laminar
$exit$	=	exit
T	=	turbulent
θ	=	circumferential direction

I. Introduction

THE range and endurance of aircraft cruising at high altitude is limited by multiple factors, including the operational efficiency of the low pressure turbine. As aircraft altitude increases, the operational Reynolds number decreases due to the change in density. The low Reynolds number causes the development of transitional and laminar flow boundary layers on the suction surface of the low pressure turbine blades. The flow is more susceptible to separation in laminar boundary layers due to the presence of adverse pressure gradients on the suction side of the blade. Boundary layer separation results in aerodynamic losses which in turn lowers engine efficiency, which reduces the aircraft range and maximum altitude. To understand how to improve designs, better capability for prediction of low Reynolds number turbine flows is needed.

The success of performance predictions of turbine stages using CFD are dependent on the ability to model loss mechanisms such as boundary layers, blade trailing edge wakes, and secondary flows. Also, interactions between adjacent blade rows cause an inherently unsteady flowfield within the turbine stages due to wake and potential effects. Wake effects are due to the shedding of boundary layer vorticity and momentum deficit by blades located upstream. Potential effects originate from unsteady variations in the pressure field that propagate both upstream and downstream. CFD simulations of multistage geometries must be able to model these effects reasonably. Fully unsteady simulations are required to accurately model these effects where the flowfield of each blade row are solved simultaneously in time-accurate manner, and meshes for blade rows that involve rotation are moved relative to stationary blade rows. This type of simulation requires a significant amount of computational resources. An alternative method is to employ a “mixing plane” model¹. The mixing plane model is a method for simulating flow through domains with one or more regions in relative motion. The fluid zone for each blade was treated as a steady state solution using circumferentially averaged or “mixed” profiles of dependent variables. The boundary profiles are updated between adjacent blade rows for each local iteration. Any unsteadiness was removed that would normally occur due to circumferential variations in the flowfield between passages, like wakes, shock waves, and separated flow. Performance predictions made using the mixing plane model have been shown to produce reasonable results^{2,3}.

The most widely used CFD method for simulations involving three-dimensional rotating turbomachinery is the Reynolds Averaged Navier-Stokes (RANS) method using statistical turbulence models. Currently, Large-Eddy Simulation or Direct Numerical Simulation CFD methods require impractically long simulation times for these types

of flows in multiple stage geometries. For RANS CFD solvers, all flow quantities are expressed as the sum of mean and fluctuating parts where the whole range of turbulent scales is computed using a simplified model. Successful modeling of low Reynolds number flows involving laminar to turbulent transition and separation has been limited when using conventional RANS turbulence models. Most conventional turbulence models assume fully turbulent flow with no transitional effects, and fail to predict separation with good accuracy.

However, several studies have been done where conventional RANS turbulence models have been modified to include transitional flow effects and separation. Choi and Yoo⁴ used the low Reynolds number form of Menter's $k-\omega$ turbulence model to study the rotor-stator interactions of a single stage axial turbine. Although the model did not predict the onset of transition or wake-induced transition properly, it did represent the general trend of the transitional flow adequately with satisfactory agreement with experimental results. Menter *et al.*⁵ used transport equations for intermittency and the momentum thickness Reynolds number. The intermittency equation was coupled with Menter's $k-\omega$ SST model and used to trigger the production of turbulent kinetic energy beyond the turbulent transition region. The second transport equation was formulated in terms of the momentum thickness Reynolds number at transition onset. An empirical correlation was used to control the transition onset criteria in the intermittency equation. Another approach by Praisner *et al.*^{6,7} used correlations developed from an experimental database for attached flow transition, laminar separation with turbulent attachment, and separated-flow transition. These correlations were implemented in a RANS solver using the Wilcox $k-\omega$ turbulence model. The model showed significant improvement in the predicted accuracy of the total pressure loss for both linear cascades and multistage LPT rigs over a conventional fully turbulent flow model.

Recently, a new three-equation eddy-viscosity type model has been developed by Walters and Leylek⁸ for modeling transitional flow effects to improve loss prediction capability using RANS solvers. Transport equations are used to address the development of pre-transitional fluctuations in the boundary layer and the breakdown to turbulence to predict both natural and bypass transition. This model has been applied to the cases of a zero-pressure-gradient flat plate at various freestream turbulent intensities by Walters and Leylek⁸ and a circular cylinder at subcritical, critical, and supercritical Reynolds numbers by Halloway *et al.*⁹ with good results. Also, the capability of the new model to predict transitional flow behavior has been demonstrated on a highly loaded turbine blade airfoil with and without film cooling and a flat plate with pressure distribution similar to an axial compressor undergoing passing wakes by Walters and Leylek^{10,11}. The intent of this new model is to provide the same ease-of-use as conventional turbulence models. It is independent of integral and non-local inputs, as well as intermittency factors.

Walters and Leylek⁸ laminar-to-turbulent transitional flow model was recently utilized by the current authors¹². The ability to adequately predict the Reynolds number effect on the total pressure loss coefficient was demonstrated for an attached transitional flow using a two-dimensional cascade CFD model of a lightly loaded blade. Also, the unsteady features of separation and vortex generation of the flowfield were qualitatively investigated for a highly loaded cascade model. Good agreement was shown with the experimental results in prediction of separation and reattachment, but quantitative inaccuracies in the size of the separation region were observed. The absence of spanwise distribution of three-dimensional structures present in separated shear layers not replicated in the two-dimensional study may have lead to inaccuracies when compared to experimental results. The $k_T-k_L-\omega$ transitional model demonstrated the potential to provide performance prediction of transitional flow for low Reynolds number airfoils.

This present study examined the flowfield of a three-dimensional multistage LPT geometry that has been subjugated to low inlet Reynolds number flow effects. CFD simulations were completed using the mixing plane calculation method in combination with the Spalart-Allmaras(S-A) turbulence model. Steady flow simulations were completed at both nominal and high altitude inlet conditions corresponding to two different inlet Reynolds numbers. The flowfield for each blade row was investigated using streamlines and surface flow visualizations at each altitude condition to identify the sources of aerodynamic losses. The total pressure loss coefficient was calculated and used as an indicator to judge aerodynamic performance. Initial work was completed with the 1st stage of the multistage LPT, investigating the ability of the Walters and Leylek⁸ laminar-to-turbulent transitional flow model to predict the boundary layer behavior and performance at low inlet Reynolds numbers. The $k_T-k_L-\omega$ model results were compared to the S-A model at the nominal altitude condition to determine the difference in the flowfield predictions each method provided. Surface flow, flowfield streamlines, and total pressure loss coefficient were used to make comparisons of the flowfield behavior. These results provided the initial step to use the $k_T-k_L-\omega$ model in conjunction with the mixing plane method for improved low inlet Reynolds numbers prediction capability for the multistage LPT geometry.

II. CFD Numerical Methods

A. Computational Grid Technique

The methodology developed in Sanders *et al.*¹² was applied to a multistage LPT geometry consisting three stator-rotor stages. A structured grid was designed for the LPT multistage geometry because of the high degree of control and accuracy with lower amount of computational memory requirement. The same grid O-H topology was used for all six blade flowpaths. The three-dimensional O-grid was made using a hyperbolic extrusion method normal to the blade surface. The first cell wall distance had a $y^+ < 1$ in accordance with the transitional model wall spacing tolerance. Typical O-grid dimensions for each blade row are given in Table 1. A cutting plane grid approximately (35×151) was constructed to control the grid point distribution within the H-grid flowpath. The hub and shroud grid surfaces approximately (333×35) were created based on the node connectors from the cutting plane, blade O-grid, and main flowpath. The elliptic structured grid solver was used so that the minimum-angle cell skewness was above 45°. This cell skewness tolerance was set to make sure the cell shape would not affect the CFD solver accuracy and performance. The grid point distribution of the H-grid boundaries was made so that periodic boundaries can be applied across the blade passage. The flowpath H-grid block dimensions for each of the six blade rows is given in Table 1 including the total number of cells for each blade row. Figure 1 shows the grid topologies for each of the three stages of the multistage LPT geometry.

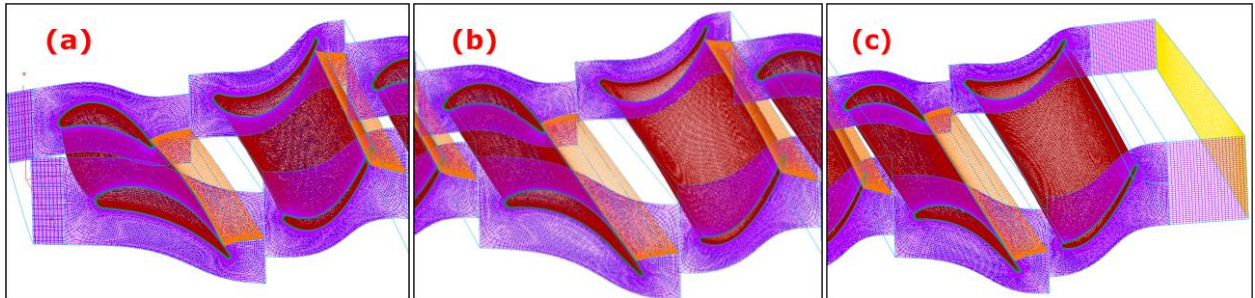


Figure 1. Structured Grid for the Multistage LPT Geometry.
(a) 1st Stage, (b) 2nd Stage, and (c) 3rd Stage Vane and Rotor

	O-Grid Dimensions	H-Grid Dimensions	Cells		O-Grid Dimensions	H-Grid Dimensions	Cells
Inlet		25×41×151	154,775	2nd Rotor	346×14×165	346×35×165	2,797,410
1st Vane	333×17×151	333×35×151	2,614,716	3rd Vane	339×18×165	339×31×165	2,740,815
1st Rotor	335×16×151	335×37×151	2,681,005	3rd Rotor	342×16×168	342×31×168	2,705,640
2nd Vane	333×17×153	333×31×153	2,445,552	Outlet		25×43×168	180,600

Table 1. Blade Row Grid Dimensions and Cell Count for Multistage LPT Geometry

Typically 151 grid points were distributed along the spanwise direction with an initial wall spacing, $\Delta s = 3.81\mu\text{m}$. A grid independence study was performed to determine if the baseline grid had enough resolution in the spanwise dimension and small enough wall spacing. A mixing plane model simulation was completed for the 1st stage of LPT multistage geometry using the Spalart-Allmaras turbulence model at the nominal altitude inlet conditions. The grid topology for the 1st stage mixing plane model consisted of a single blade row of the 1st stage vane and rotor with an outflow region extended 0.5in in the axial direction. The outflow region contains 139,524 cells in two (21×22×151) blocks. The baseline grid of the 1st stage mixing plane model contained 5,315,100 cells. The number of spanwise grid-points were increased by 50% for the baseline grid with an initial wall spacing, $\Delta s = 0.76\mu\text{m}$, to create the finer mesh while maintaining the same axial and tangential grid-point distribution for the blade surface and the main flowpath. The total number of grid-points for the fine grid was 8,082,664 cells. The comparison of the wall y^+ for the baseline and fine grid of the 1st stage blade, hub and shroud surfaces is shown in Figure 2. The grid comparison study is discussed in the Grid Independence Study Results Section.

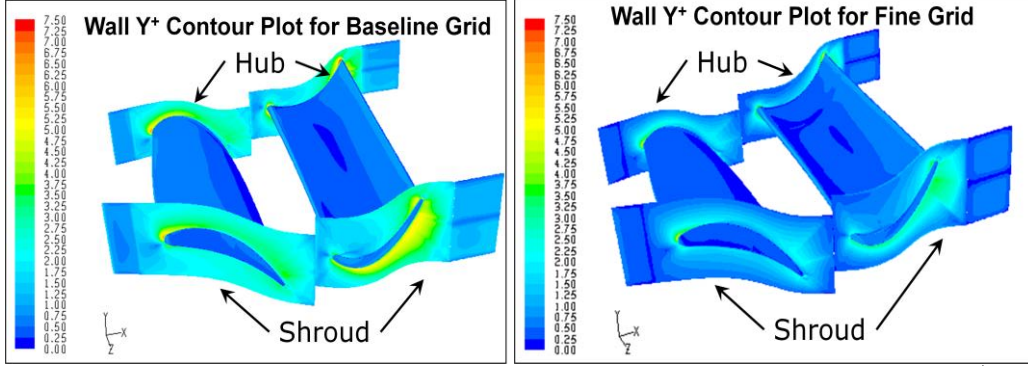


Figure 2. Comparisons of the Wall y^+ Contour Plot for the Baseline and Fine Grid 1st Stage Mixing Plane Model of the Multistage LPT Geometry

B. CFD Numerical Scheme

CFD simulations were performed using ANSYS Fluent 6.3[®] which is based on a finite volume method. The domain was discretized onto a finite set of control volumes and the general conservation equations mass, momentum, and energy, were solved on this set of control volumes. The partial differential equations based on the RANS equations shown in Eq. (1-3) were discretized algebraically and solved for the mapping of the flowfield.

$$\frac{\partial \rho}{\partial t} + \frac{\partial}{\partial x_i}(\rho u_i) = 0 \quad (1)$$

$$\frac{\partial}{\partial t}(\rho u_i) + \frac{\partial}{\partial x_j}(\rho u_i u_j) = -\frac{\partial p}{\partial x_i} + \frac{\partial}{\partial x_j} \left[\mu \left(\frac{\partial u_i}{\partial x_j} + \frac{\partial u_j}{\partial x_i} - \frac{2}{3} \delta_{ij} \frac{\partial u_k}{\partial x_k} \right) \right] + \frac{\partial}{\partial x_j}(-\rho \overline{u'_i u'_j}) \quad (2)$$

$$\frac{\partial}{\partial t}(\rho C_p T) + \frac{\partial}{\partial x_j} \left(\rho C_p u_j T - k \frac{\partial T}{\partial x_j} \right) = \frac{\partial P}{\partial t} + u_j \frac{\partial P}{\partial x_j} + \mu \left(\frac{1}{2} \left[\frac{\partial u_i}{\partial x_j} + \frac{\partial u_j}{\partial x_i} \right]^2 - \frac{2}{3} \left[\frac{\partial u_k}{\partial x_k} \right]^2 \right) \quad (3)$$

All solution variables represent ensemble or time averaged values. The Reynolds stress term $-\rho \overline{u'_i u'_j}$ is resolved according to the chosen turbulence model in order to close the equation. The RANS equations were discretized using the pressure-based coupled algorithm which solved a coupled system of equations comprising the momentum and energy equations with the pressure-based continuity equation. The convergence rate significantly improved when compared to the pressure-based segregated algorithm.

The mixing plane model is a method for simulating flow through domains with one or more regions in relative motion. The fluid zone for each blade was treated as a steady state solution. The flowfield parameters from adjacent zones were passed as boundary conditions that were spatially averaged at the mixing plane interface. Any unsteadiness was removed that would normally occur due to circumferential variations in the flowfield between passages, like wakes, shock waves, and separated flow. Mass-weighted averages in the circumferential direction at specified radial locations or profiles of flow properties were used to update boundary conditions along the two mixing plane interface zones. A mixing plane interface was made between an upstream outlet boundary zone and downstream inlet boundary zone.

This type of model provided several computational advantages by giving a steady-state approximation to the time-averaged flowfield at a reduced computational solution completion time. Unsteady calculations involving rotation require significant amount of computational time to achieve a time-periodic solution. The mixing plane model does not require a common periodic angle to be maintained for each blade row. This allowed a geometry configuration of one blade passage per row without modifying the blade count. So, the modeling of a large amount of blade passages was avoided which reduced the overall grid size. In addition, the grid for each blade inlet and exit boundaries does not have to be conformal and can be of different types (i.e., vane can be an unstructured grid while downstream blade can be a structured grid).

C. Solution Convergence Procedure

The numerical scheme used in the mixing plane model simulations using the Spalart-Allmaras turbulence model were initialized based on the inlet boundary conditions in the absolute frame of reference with a first-order upwind scheme for density, turbulence, and pressure with a second-order upwind discretization scheme for energy and momentum. Several hundred iterations were performed with turbulence and energy equations disabled to help establish the main flowfield after which the turbulence and energy equations were re-enabled, respectively. Once solution stability was achieved, the CFL was increased to speed the local time stepping while maintaining stability. The solutions were run until convergence tolerance of 10^{-5} for global flow variables was reached. Second-order upwind discretization for all flow parameters and equations were set and were ran again until convergence tolerance of 10^{-5} for global flow properties was achieved.

A specific solution convergence procedure using Walters and Leylek's transitional flow model was developed in order to maintain solution stability and prevent divergence. A converged solution using the k - ε model was ran with second-order upwind numerical scheme in order to provide an initial approximation of the flowfield. The k_T - k_L - ω model was enabled and ran sequentially with the first and second-order upwind numerical scheme until convergence of 10^{-5} global flow properties was reached. The flowfield was held "frozen" by disabling the continuity, momentum, and energy equations during this process. The frozen flow solution was used as the initial condition while all equations including continuity, momentum, and energy were re-enabled with k_T - k_L - ω model equations and ran sequentially with the first and second-order numerical scheme. The same residual convergence tolerance of 10^{-5} was attained for all simulations using the k_T - k_L - ω model.

D. Spalart-Allmaras Turbulence Model

The Spalart-Allmaras model is a one-equation turbulence model specifically developed for aerodynamic external flow applications. It uses a single transport equation for the eddy viscosity. The model was developed to remove the incompleteness of algebraic and one-equation turbulent kinetic energy models and yet more computationally simple than more advanced turbulence models. Overall the Spalart-Allmaras model performs well for transonic and mildly separated flows and widely used in turbomachinery applications although, its accuracy is known to suffer for flows with massive separation and free shear flows. The model equations are based on the transport of a parameter proportional to the turbulent viscosity given in Eq. (4)-(5)

$$\mu_t = \rho \tilde{\nu} f_{v1} \quad (4)$$

$$\rho \frac{D\tilde{\nu}}{Dt} = \rho c_{b1} \tilde{S} \tilde{\nu} + \frac{1}{\sigma_{\tilde{\nu}}} \left[\frac{\partial}{\partial x_j} \left\{ (\mu + \rho \tilde{\nu}) \frac{\partial \tilde{\nu}}{\partial x_j} \right\} + c_{b2} \rho \left(\frac{\partial \tilde{\nu}}{\partial x_j} \right)^2 \right] - c_{w1} \rho f_w \left(\frac{\tilde{\nu}}{d} \right)^2 \quad (5)$$

A full description of all the model constants and source terms are discussed in Wilcox¹³.

E. Walters and Leylek's Transitional Flow Model

The Walters and Leylek's k - k_L - ω model is a three-equation eddy-viscosity type, with transport equations for the turbulent kinetic energy (k_T), laminar kinetic energy (k_L), and the specific dissipation rate (ω) which are given in Eqs. (6)-(8).

$$\frac{Dk_T}{Dt} = P_{k_T} + R + R_{NAT} - \omega k_T - D_T + \frac{\partial}{\partial x_j} \left[\left(\nu + \frac{\alpha_T}{\sigma_k} \right) \frac{\partial k_T}{\partial x_j} \right] \quad (6)$$

$$\frac{Dk_L}{Dt} = P_{k_L} - R - R_{NAT} - D_L + \frac{\partial}{\partial x_j} \left[\nu \frac{\partial k_L}{\partial x_j} \right] \quad (7)$$

$$\frac{D\omega}{Dt} = P_\omega + C_{\omega R} \frac{\omega}{k_T} (R + R_{NAT}) - C_{\omega 2} \omega^2 - C_{\omega 3} f_\omega \alpha_T \left(\frac{\lambda_{eff}}{\lambda_T} \right)^{4/3} \frac{\sqrt{k_T}}{d^3} + \frac{\partial}{\partial x_j} \left[\left(\nu + \frac{\alpha_T}{\sigma_\omega} \right) \frac{\partial \omega}{\partial x_j} \right] \quad (8)$$

The influence of the laminar and turbulent kinetic energy on the Reynolds stress term was included through the prescription of the total eddy viscosity as given in Eq. (9). A brief summary of the current transitional flow model functionality is presented below.

$$-\overline{u'_i u'_j} = \nu_{TOT} \left(\frac{\partial u_i}{\partial x_j} + \frac{\partial u_j}{\partial x_i} \right) - \frac{2}{3} k_{TOT} \delta_{ij} \quad (9)$$

The laminar kinetic energy was used to describe the low frequency, high amplitude fluctuations that originated from the pre-transitional boundary layer. These fluctuations primarily occurred at one scale and almost all energy was contained in a single streamwise component. The production of laminar kinetic energy was assumed to occur due to a ‘‘splat mechanism’’ which redirected the normal fluctuations of the freestream turbulence into a streamwise component while creating local pressure gradients in the boundary layer, thus increasing the low frequency fluctuations. These fluctuations grow to the development of turbulent spots and then to full turbulence. A local transition parameter that depended on the turbulent energy, effective length scale, and fluid viscosity determined when this occurred. Once this parameter reached a threshold value, a transfer of energy began from streamwise fluctuations (k_L) to turbulent fluctuations (k_T).

Both natural, mixed, and bypass transition were resolved in the current model. Natural transition occurred when orderly laminar flow broke down to turbulent flow in presence of small perturbations. This process was very slow and was observed when no external forcing was applied and when very small perturbations were present. Bypass transition evolved when those perturbations were large enough to bypass the exponential growth of Tollmien-Schlichting (TS) waves. The mixed transition regime involved elements of both natural and bypass transition. The production terms in the current model controlled the transfer from streamwise fluctuations to full turbulence which depended on the laminar kinetic energy and the local mean velocity in order to include natural and mixed transition. A full description of all model variables and dependences were presented by Walters and Leylek⁸.

F. Boundary Conditions

The CFD boundary conditions for the mixing plane model were set to simulate the actual engine operation at both nominal and high altitude conditions. Inlet conditions to the 1st stage vane were based on the typical inlet profiles seen by multistage LPT. Radial variations of the total pressure, total temperature, and tangential and radial flow angles were specified with an estimated inlet static pressure. The radial and tangential flow angles were converted to directional velocity components using spherical coordinate transforms. The initial inlet turbulent viscosity ratio was set as $\mu_t/\mu = 7.364$ for all simulations, and an inlet turbulent intensity, $Tu = 1\%$ was set for only the k_T - k_L - ω model simulations. The initial outlet static pressure was defined with a radial equilibrium pressure distribution using Eq. 10.

$$\frac{\partial P}{\partial r} = \frac{\rho v_\theta^2}{r} \quad (10)$$

was set for the pressure outlet boundary condition to determine the radial distribution of the back pressure. The fluid zone for the rotor stages were set in the moving reference frame with a rotational speed with respect the x-axis direction, while the vane fluid zones were set in the stationary or absolute reference frame. The blade speeds for the nominal and high altitude conditions were 7700 rpm and 7900 rpm, respectively. All hub and shroud endwalls and blade surfaces were set as stationary no-slip walls relative to the motion of its adjacent fluid zone. The mixing plane interface zones placed between inlet and exit of each blade row used a 151 point radial profile for circumferential averaging. Periodic boundary conditions were assigned to the mid-passage flow boundaries to model the approximate time-averaged operation of a full annulus blade row.

III. Grid Independence Study Results

The mass-weighted averaged total pressure and total temperature at the 1st vane and 1st rotor inlet and outlet were compared to the baseline and fine grid. All mass-weighted quantities were normalized using the maximum value for the stage. Figure 3 shows a similar total pressure and total temperature ratio across the 1st vane and 1st rotor for the fine and baseline grid. The baseline and fine grid also showed a similar loss coefficient distribution across the 1st vane and rotor in Figure 3. The loss coefficient was calculated with Eq. (11) by taking the difference between the inlet and exit total pressure and dividing by the difference between the mass-weighted averaged inlet total and static pressure.

$$TPLC = \frac{(P_{0,in} - P_{0,exit})}{(P_{0,in} - P_{in})} \quad (11)$$

The results indicated that the baseline and fine grid showed a similar loss coefficient distribution across the 1st vane and rotor. This indicated the baseline grid provides adequate resolution of the spanwise flowfield and sufficient initial spacing for endwall effects. Each blade row of the multistage LPT geometry was similar in grid topology as the baseline grid.

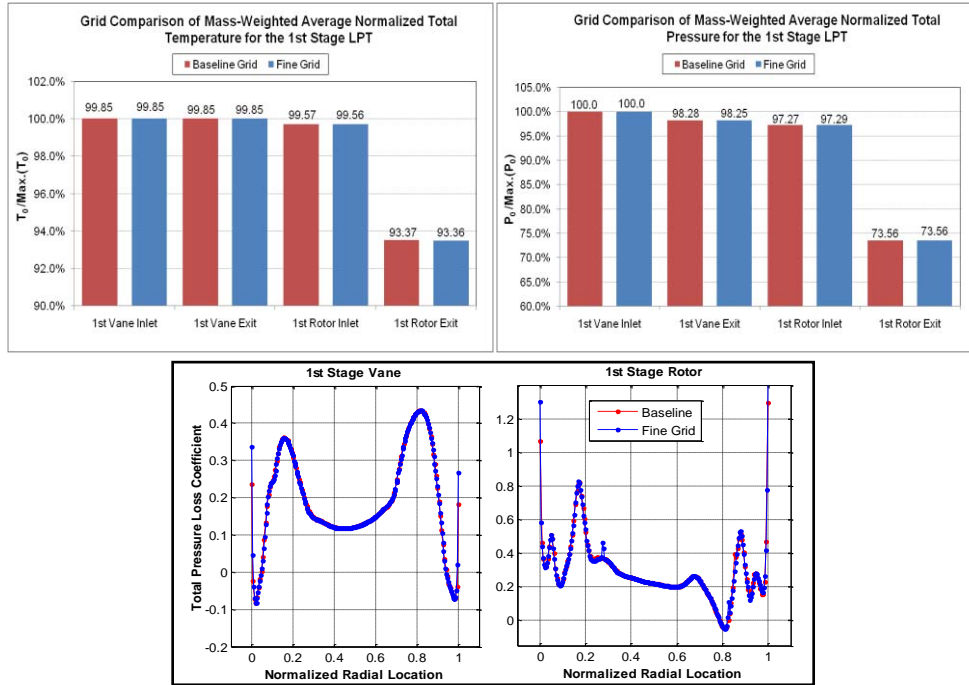


Figure 3. Comparison of the Mass-Weighted Average Total Temperature, Total Pressure, and Efficiency for the Baseline and Fine Grid.

IV. Flowfield Comparisons at the Nominal and High Altitude Conditions

The low Reynolds number flow effects were investigated using a multistage LPT geometry. Table 2 shows the decrease in the inlet Reynolds number multistage LPT geometry compared to the nominal and high altitude condition. These calculations were based on mass-weighted averages of fluid flow properties. The Reynolds number was calculated using the mid-radius true chord as the characteristic length. The Spalart-Allmaras turbulence model was used in simulations at both altitude conditions. Comparisons were evaluated based on flowfield visualizations using surface flow, flowfield streamlines, and the total pressure loss coefficient for each stage.

	Altitude Condition	Inlet Re No.		Altitude Condition	Inlet Re No.
1 st Stage Vane	Nominal	135,000	2 nd Stage Rotor	Nominal	108,000
	High	20,000		High	16,000
1 st Stage Rotor	Nominal	123,000	3 rd Stage Vane	Nominal	85,000
	High	19,000		High	12,000
2 nd Stage Vane	Nominal	110,000	3 rd Stage Rotor	Nominal	86,000
	High	16,000		High	12,000

Table 2. Inlet Reynolds Numbers for each Blade Row at Nominal and High Conditions

A. Streamlines and Surface Flow Visualizations

Streamlines and surface flow visualizations were created in order to help visualize any vortical structures present in the flowfield for each stage. The presence of these vortical structures was used as an indicator of sources of aerodynamic losses which cause an increase in the total pressure loss coefficient for each blade row. All visualizations were created using FIELDVIEW[®] CFD visualization software. The streamlines were created by arbitrarily placing seed points on iso-surfaces based on a constant value of the Mach number. The seed points were

used to calculate the particle paths by integrating through the velocity vector using a second order Runge-Kutta method. Surface flows are defined as special streamlines which are restricted to lie in the plane of the blade surface. The surface streamlines were calculated using the velocity gradient on the surface.

1st Stage

Figure 4 shows the comparison of surface flow and flowfield streamlines for the 1st stage vane at the nominal and high altitude condition. The surface flow results for the S-A model (Fig. 4(a)) revealed that the flow from the endwalls moved toward the blade mid-span and met the main streamwise flow which resulted in a foci of separation near the trailing edge of the suction surface. Similar secondary flow effects were observed in the vane for each stage. Downstream of the separation point, two large vortices located at 10% and 75% the blade span are clearly evident. A third small counter-clockwise vortex close to the shroud endwall is also apparent as shown in Fig. 4(b). The surface flow results in Fig. 4(c) at the high altitude condition show that main foci of separation was located more upstream on the suction surface than the nominal altitude result. The flowfield streamlines in Fig. 4(d) revealed the flow was largely separated along the entire blade span. Also, the vortical structures identified at nominal altitude condition have increased in size. The order of magnitude decrease in the inlet Reynolds number at the high altitude condition was attributed to the increase in the separation present for all blade rows within each stage.

Both the nominal and high altitude condition showed similar surface flow and flowfield streamline patterns as indicated in Figure 5 for the 1st stage rotor. The surface flow patterns (Fig. 5(a) & Fig. 5(c)) indicated that the streamwise flow separated from the blade pressure surface at the leading edge and reattached to the blade surface further downstream. The leading edge separation and reattachment positions were located at similar relative position on the pressure surface. Also, a saddle point was present indicating the presence of small vortical structures near both endwalls. Figures 5(b) and 5(d) show the structure of the recirculation region as a result of the leading edge separation and reattachment. Also, smaller vortical structures were observed close to the hub surface. There was not any evidence of separation present on the 1st stage rotor suction surface for either altitude condition.

2nd Stage

The flow remained mostly attached to surface for the majority of the 2nd stage vane span at the nominal altitude condition (Fig. 6(a)). Surface flow pattern showed very small vortical structures at 10% of the span near the hub surface and 85% of the blade span. The streamlines in Fig. 6(b) reveal the formation of the vortex close to the hub surface in greater detail. There were two distinct clockwise vortices being formed. The vortex located the closest to the hub surface eventually formed a trailing edge horseshoe vortex. In contrast, the high altitude condition showed foci of separation present on the suction surface in Fig. 6(c) with a large separation region present along a major portion of the blade surface (Fig 6(d)). This could be due to the flow from endwalls having a higher momentum than the main flow from the blade leading edge, causing the main flow to separate from the surface. Also, the vortical structure located close hub surface has increased in relative size from the nominal altitude result. Figure 8 compares the surface flow results for the 2nd stage rotor for both altitude conditions. Both results show a similar behavior of the presence of a recirculation region on the pressure surface. The high altitude condition (Fig. 8(b)) revealed the boundary layer reattachment position was found more downstream than what was observed in the nominal altitude condition (Fig. 8(a)). The increase in the amount to separation caused the reattachment position to move downstream which is mainly due to the decrease in inlet Reynolds number.

3rd Stage

Surface flow results at the nominal altitude condition shown in Fig. 7(a) for 3rd stage vane indicated separation on the suction surface due to secondary flow effects. A small vortex located close to the hub surface is shown in the flowfield streamline result in Fig. 7(b). Also, a horseshoe vortex was clearly present due to the suction surface separation. The high altitude result revealed the presence of a localized separation and reattachment region relatively close to the leading edge on the suction surface as seen in Fig 7(c). Also, there was foci of separation that was located significantly more upstream on the blade surface than the nominal altitude condition result in Fig 7(a). The flowfield streamlines (Fig. 7(d)) indicated the separated flow region extended the entire blade span. Surface flow comparison at the nominal and high altitude condition for the 3rd stage rotor shown in Fig. 9(a) and Fig. 9(b), respectively. The separation and reattachment region was located more downstream of the pressure surface in the high altitude condition, although the separation and reattachment region extends further along the blade span. The decrease in Reynolds number largely affected the flowfield in the 3rd stage vane compared to the rotor. This trend was found in all stages and suggests that improvements could be made to the vane in order to control separation and improve efficiency.

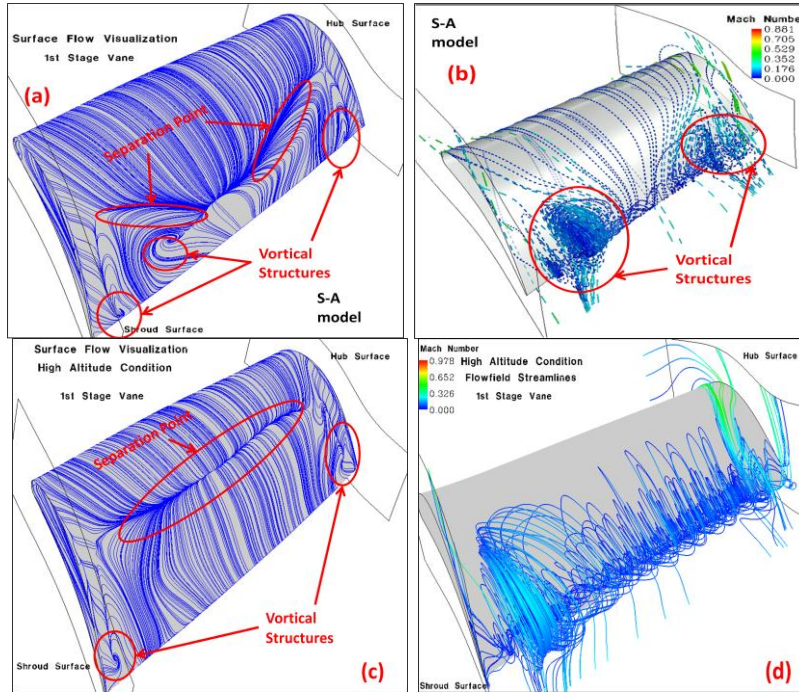


Figure 4. Spalart-Allmaras Model Comparison of the Streamlines and Surface Flow Visualization for the 1st Stage Vane. (a)Surface flow and (b)Flowfield Streamlines at the Nominal Altitude Condition, (c)Surface flow and (d)Flowfield Streamlines at the High Altitude Condition

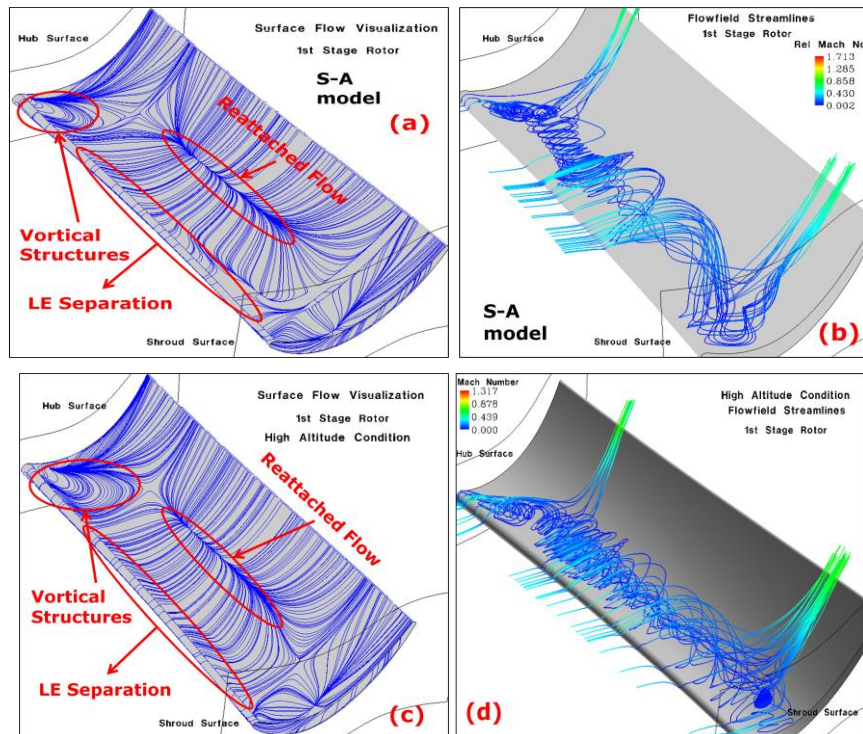


Figure 5. Spalart-Allmaras Model Comparison of the Streamlines and Surface Flow Visualization for the 1st Stage Rotor. (a)Surface flow and (b)Flowfield Streamlines at the Nominal Altitude Condition, (c)Surface flow and (d)Flowfield Streamlines at the High Altitude Condition

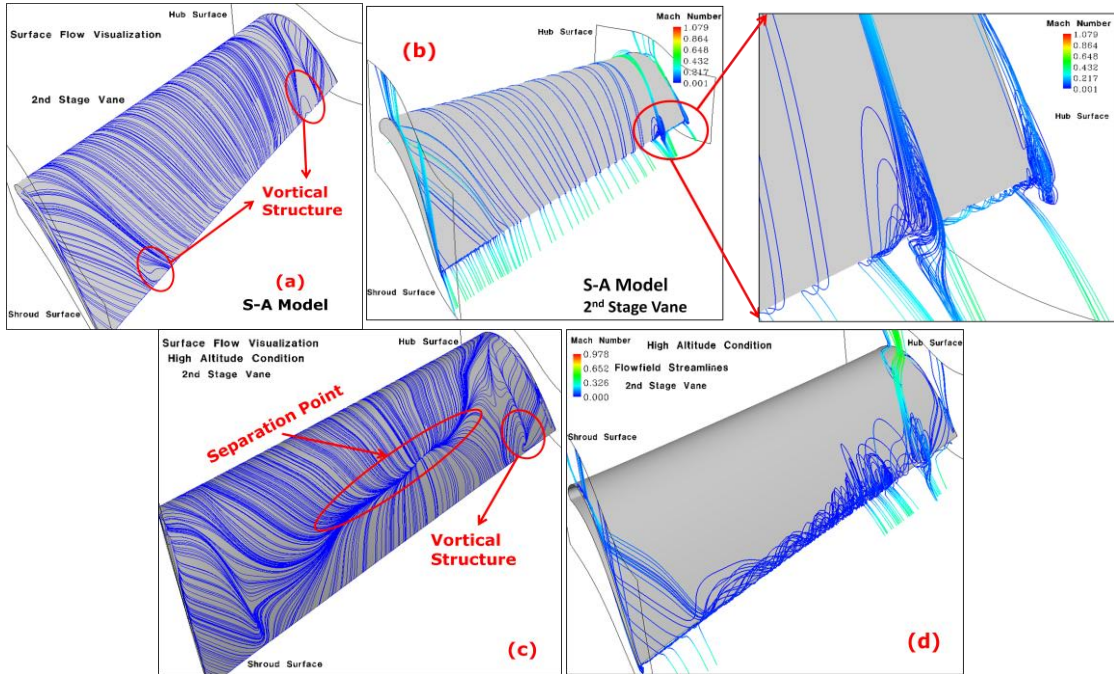


Figure 6. Spalart-Allmaras Model Comparison of the Streamlines and Surface Flow Visualization for the 2nd Stage Vane. (a)Surface flow and (b)Flowfield Streamlines at the Nominal Altitude Condition, (c)Surface flow and (d)Flowfield Streamlines at the High Altitude Condition

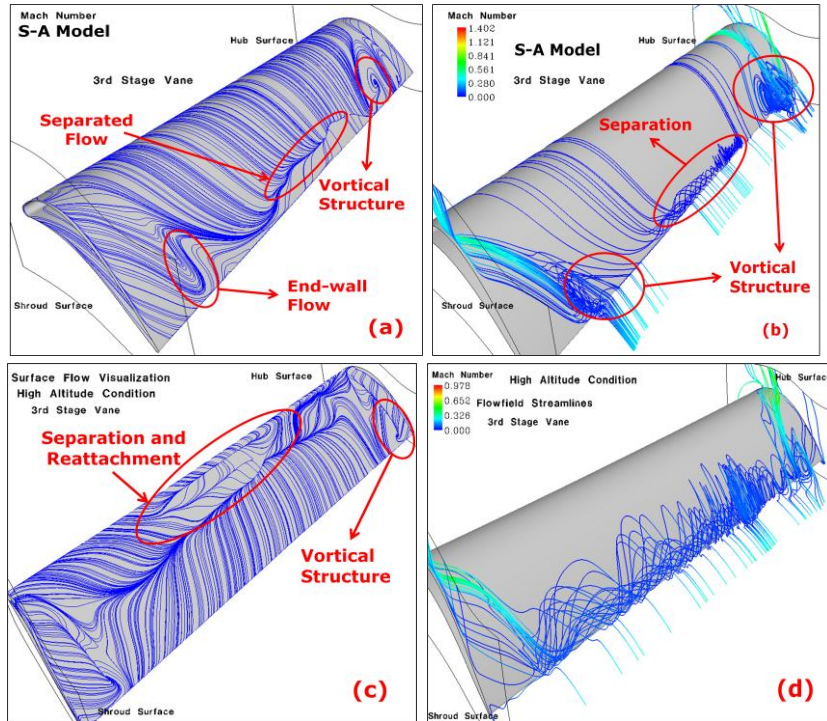


Figure 7. Spalart-Allmaras Model Comparison of the Streamlines and Surface Flow Visualization for the 3rd Stage Vane. (a)Surface flow and (b)Flowfield Streamlines at the Nominal Altitude Condition, (c)Surface flow and (d)Flowfield Streamlines at the High Altitude Condition

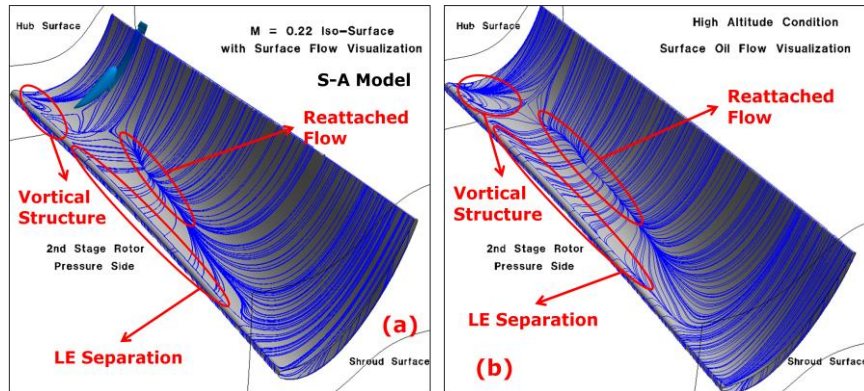


Figure 8. Spalart-Allmaras Model Comparison of the Surface Flow Visualization for the 2nd Stage Rotor. Surface flow at the (a) Nominal and (b) High Altitude Condition

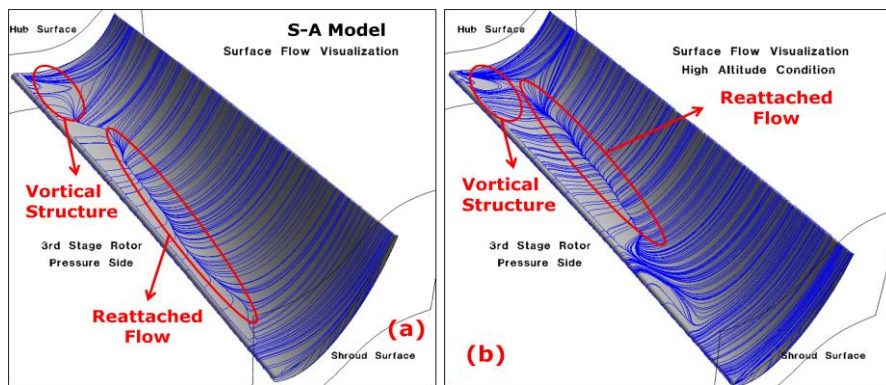


Figure 9. Spalart-Allmaras Model Comparison of the Surface Flow Visualization for the 3rd Stage Rotor. Surface flow at the (a) Nominal and (b) High Altitude Condition

B. Total Pressure Loss Coefficient Comparisons at Both Altitude Conditions

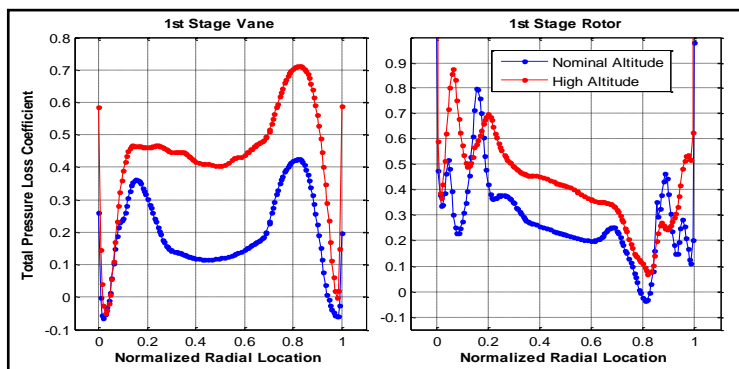


Figure 10. S-A Model Comparison of the Circumferentially Averaged Relative Total Pressure Loss Coefficient for the 1st Stage at the Nominal and High Altitude Condition

causes a reduction in the outlet relative total pressure at the exit plane. This led to a higher loss coefficient where the vortical structures and the endwalls were located. The loss coefficient is much higher relative to the 1st stage rotor than compared to the 1st stage vane. The circumferential averaged wake from the upstream vane calculated by the mixing plane method caused a significant amount of total pressure loss. Additional, the contributed total pressure loss from the secondary flow found in the rotor caused much higher loss coefficient seen in the 1st stage rotor. The higher altitude condition produced an overall higher loss for all stages due to the increase in separated flow. The large vortex present on the 1st stage vane surface showed peak increase of approximately 75% compared to the

1st Stage

The circumferential averaged total pressure loss coefficient was calculated for both the 1st stage vane and rotor (Figure 10) to determine the effect caused by vortical structures produced by the secondary flow. The loss coefficient was plotted as a function of the normalized radial location from the hub to the shroud surface. The peaks in the loss coefficient predicted from the S-A model were due to the suction side vortical structures and the endwalls from the hub and shroud for the 1st stage vane. The presence of vortical structures on the pressure side of the 1st rotor, along with the endwall effects,

nominal altitude condition with a 97% increase in the mass-weighted average loss coefficient. The loss coefficient results for the 1st stage rotor indicated the peaks due to the vortical structures have moved closer to the hub and shroud surface which could be attributed to change in the radial flow angle. The increase in the mass-weighted averaged loss coefficient was 54% for the rotor due to the decrease in Reynolds number.

2nd Stage

The total pressure loss coefficient plots for the 2nd stage are shown in Figure 11. The results for the 2nd stage vane showed the loss coefficient peaks present near the hub at both altitude conditions was due to the smaller vortex seen in the 2nd stage vane (Fig. 6(b) and 6(d)). The smaller peak close the shroud surface formed as a result of the endwall flow observed in Fig. 6(a) and Fig. 6(c). The loss coefficient results for the 2nd stage rotor revealed smaller peaks due to the smaller vortical structures located close to the each endwall surface. At the high altitude condition, the radial distribution of the loss coefficient was very similar to the nominal altitude condition. The single difference observed between the results was an approximate 62% and 68% increase in the mass-weighted averaged loss coefficient for the 2nd stage vane and rotor, respectively.

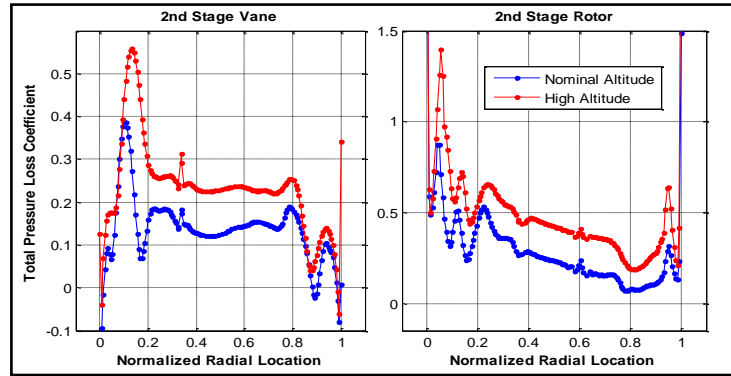


Figure 11. S-A Model Comparison of the Circumferentially Averaged Relative Total Pressure Loss Coefficient for the 2nd Stage at the Nominal and High Altitude Condition

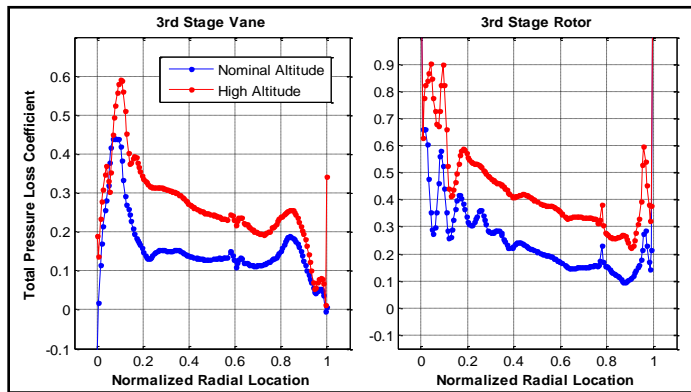


Figure 12. S-A Model Comparison of the Circumferentially Averaged Relative Total Pressure Loss Coefficient for the 3rd Stage at the Nominal and High Altitude Condition

3rd Stage

In Figure 12, the loss coefficient plot for the 3rd stage vane showed peaks near the hub surface due to the vortical structures identified in Fig. 7(a) and Fig. 7(c) for both altitude conditions. The high altitude result showed a 63% increase in the mass-weighted averaged loss coefficient as the result of the vortex present close to the hub surface. For the 3rd stage rotor, several smaller vortices were present, causing more localized loss coefficient peaks. The same trend was observed at the high altitude condition as in the 2nd stage rotor where the same radial distribution of the loss coefficient was similar to the nominal altitude condition with an increase in the mass-weighted averaged loss coefficient of 75%.

V. Turbulence Model Comparisons of the 1st Stage at the Nominal Altitude Condition

A. Streamlines and Surface Flow Visualizations

Figure 13(a) and 13(b) shows surface flow and flowfield streamlines for the 1st stage using the $k_T-k_L-\omega$ model. Surface flow results for the 1st stage vane showed the foci of separation was further upstream than observed in S-A model in Fig. 4(a). A large recirculation region was present on the suction surface due to the joining of the streamwise and endwall flow as shown in Fig 13(b). The distinct vortical structures predicted with the S-A model was not observed in the $k_T-k_L-\omega$ model results. This could be due to the inherent differences in the turbulence model equations. The S-A model assumed the flowfield to be fully turbulent, so the higher level of instabilities could be causing the flow from the endwall to form into distinct vortical structures. The $k_T-k_L-\omega$ model took into account transitional flow effects, so the turbulence generated in the flowfield grows from high amplitude streamwise fluctuations. The amount of turbulence produced in the flowfield was much less compared to the S-A model. Those

vortical structures were not present in the $k_T-k_L-\omega$ model prediction due to this dampening effect of the production of turbulence.

Both the $k_T-k_L-\omega$ (Fig. 13(c)-(d)) and S-A model (Fig. 4(c)-(d)) showed a similar surface flow and flowfield streamline patterns for the 1st stage rotor. The S-A model predicted a relatively large reattachment region, whereas the $k_T-k_L-\omega$ model predicted a tighter streamwise region of separation that rolled up and was directed outward in the radial direction. Both models predicted a saddle point behavior in the flow near the endwalls. This is more evident in the S-A model witnessed by small vortical structures close to the hub surface and the presence of the small vortical structures indentified in Fig. 4(c). These vortical structures were not observed in the $k_T-k_L-\omega$ model results with no evidence of separation present on the 1st stage rotor suction surface.

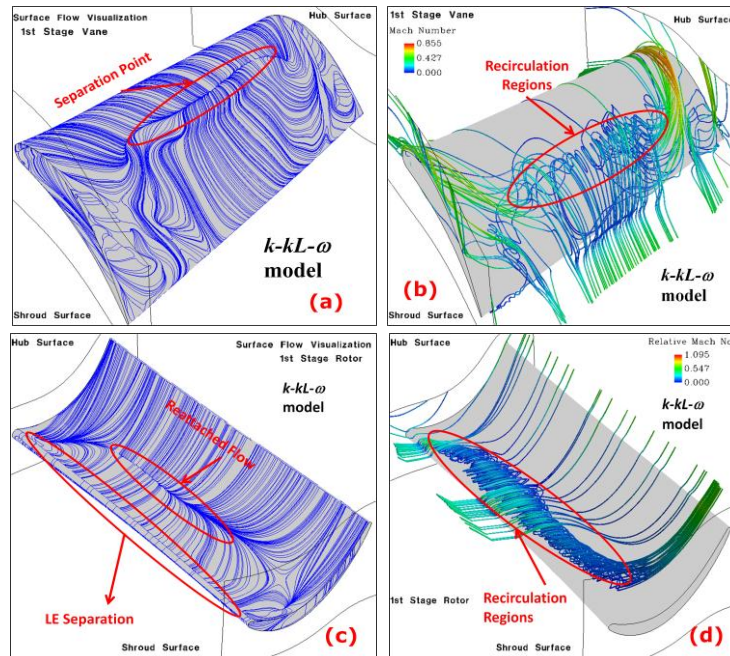


Figure 13. Streamlines and Surface Flow Visualization for the 1st Stage at the Nominal Altitude Condition using the $k-k_L-\omega$ Model. (a) Surface flow and (b) Flowfield Streamlines of the 1st Stage Vane. (c) Surface flow and (d) Flowfield Streamlines of the 1st Stage Rotor

B. Total Pressure Loss Coefficient Comparison

The circumferential averaged total pressure loss coefficient was calculated for both the 1st stage vane and rotor (Figure 14) to determine the effect the secondary flow on the total pressure loss coefficient. The peaks in the loss coefficient predicted from the Spalart-Allmaras model were due to the suction side vortical structures and the endwalls from the hub and shroud. The presence of vortical structures on the pressure side of the 1st rotor, along with the endwall effects, causes a reduction in the outlet relative total pressure at the exit plane. This led to a higher loss coefficient at the location of the vortical structures and the endwalls.

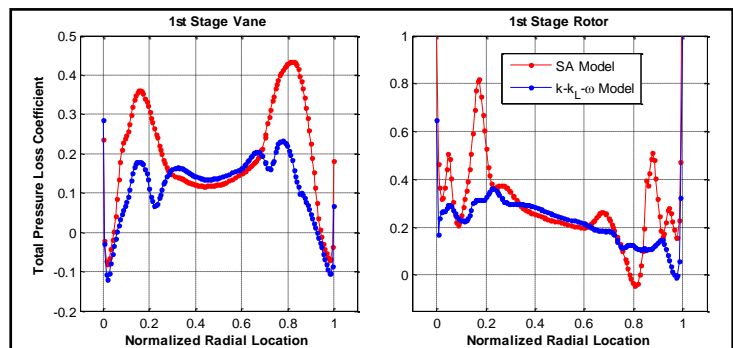


Figure 14. Turbulence Model Comparison of the Circumferentially Averaged Relative Total Pressure Loss Coefficient for the 1st Stage at the Nominal Altitude Condition

The loss coefficients results predicted with $k_T-k_L-\omega$ transitional flow model showed a reduction in the loss coefficient compared to Spalart-Allmaras model for both the 1st stage vane and rotor. This was due to the absence of the vortical structures in both blade rows that were first observed with Spalart-Allmaras model. This over-prediction

in the loss coefficient using conventional turbulence models such as the Spalart-Allmaras model has been observed by the authors and reported previously¹². This is the inherent limitation with conventional RANS turbulence models in the inability to account for transitional flow effects at low inlet Reynolds numbers.

VI. Conclusions

The operational efficiency of low pressure turbines operating at high altitudes is known to decrease due to the reduction of the operational Reynolds number. The low Reynolds number causes an increase in aerodynamic losses due to the development of laminar flow separation. CFD predictions need to demonstrate accurate modeling of laminar-turbulent boundary layer transition in order to predict the resulting aerodynamic performance from low Reynolds number effects. Flows in a multistage LPT geometry were simulated at nominal and high altitude conditions corresponding to an order of magnitude decrease in the Reynolds number. The Spalart-Allmaras turbulence model was used in combination with the mixing plane CFD technique to approximate the time-averaged flowfield using a steady-state simulation. Surface flow and flowfield streamline visualization was used to investigate vortical structures present within the flowfield as sources of aerodynamic losses. The results indicated the higher altitude condition had significant more separated flow than nominal altitude condition. The vane for each stage had significantly more separated flow compared to the rotor blades. The flowfield behavior was similar in the rotor blades for each stage, which could be attributed to the treatment of wake effects from the upstream vane by the mixing plane method. Also, the circumferentially-averaged total pressure loss coefficient was calculated for each blade row and compared at both altitude conditions. The 1st stage vane was shown to have largest secondary flow present within its flowfield causing the 1st stage rotor to have a larger peak total pressure loss than any of the other blade rows at the nominal altitude condition. At the high altitude condition, the 2nd stage rotor was observed to have the largest peak total pressure due to the large vortex present in the upstream vane. The results suggested if the separated flow found in the vane for each stage can be reduced, the total pressure loss in the rotor blade can be reduced resulting in an increased efficiency for the stage at the higher altitude condition.

A new three-equation eddy-viscosity type turbulent transitional flow model developed by Walters and Leylek⁸ was used in simulations for the 1st stage of the multistage LPT geometry. The results were compared to those obtained with the Spalart-Allmaras turbulence model at the nominal altitude condition. The large vortices predicted in the Spalart-Allmaras model results were not observed in the $k_T-k_L-\omega$ model results. This can be attributed to the dampening of the amount turbulence produced within the flowfield, thus reducing the generation of vortical structures. In a previous investigation by Sanders *et al.*¹², the loss coefficient results were over-predicted with the Spalart-Allmaras model for both the 1st stage vane and rotor. Since the $k_T-k_L-\omega$ model accounts for transitional flow effects, it might provide a more accurate method for performance predictions compared to conventional RANS turbulence models. Future work will consist of completing simulations with the Walters and Leylek⁸ transitional flow model for the full multistage LPT geometry at both altitude conditions.

Acknowledgments

The work presented was sponsored by the Air Force Research Laboratory, Propulsion Directorate, Turbine Engine Division. Computing resources were provided by the U.S. Department of Defense Major Shared Resource Center, High Performance Computing facility at Wright Patterson AFB, OH. The authors are grateful to H. Thornburg for assistance with mesh generation and helpful discussions. Also, C. Hah from NASA Glenn Research Center and F. Kelecý from ANSYS[®] are acknowledged for their helpful advice with CFD simulation set-up and analysis.

References

- ¹Dawes, W.N., "Towards Improved Throughflow Capability: The Use of 3D Viscous Flow Solvers in a Multistage Environment", ASME Journal of Turbomachinery, Vol. 114, January 1992, pp 8–17.
- ²Dorney, D.J., and Sharma, O.P., "Evaluation of Flow Field Approximations for Transonic Compressor Stages", ASME Journal of Turbomachinery, Vol. 119, July 1997, pp 445–452.
- ³Wiess, J.M., and Kelecý, F.J., "Numerical Simulation of Steady-State Flow Through a Multi-Stage Turbine using Unstructured Meshes" ASME Paper No. FEDSM-99-6862.
- ⁴Choi, C.H., and Yoo, J.Y., "Unsteady Blade-Row Flow Calculations Using a Low-Reynolds-Number Turbulence Model", Journal of Propulsion and Power, Vol. 16, No. 5, Sept. - Oct. 2000.

- ⁵ Menter, F.R., Langtry, R.B., Likki, S.R., Suzen, Y.B., Huang, P.G., and Volker, S., “A Correlation-Based Transition Model Using Local Variables- Part I: Model Formulation”, *Journal of Turbomachinery*, Vol. 128, July 2006, pp 413 – 422.
- ⁶ Praisner, T.J., and Clark, J.P., “Predicting Transition in Turbomachinery, Part I – A Review and New Model Development”, ASME Paper No. GT-2004-54108.
- ⁷ Praisner, T.J., Grover, E.A., Rice, M.J., and Clark, J.P., “Predicting Transition in Turbomachinery, Part II – Model Validation and Benchmarking”, *Journal of Turbomachinery*, Vol. 129, January 2007, pp 14 – 22.
- ⁸ Walters, D.K., and Leylek, J.H., “A New Model for boundary Layer Transition Using a Single Point RANS Approach”, *Journal of Turbomachinery*, Vol. 126, January 2004, pp 193–202.
- ⁹ Holloway, D.S., Walters, D.K., and Leylek, J.H., “Prediction of Unsteady, Separated Boundary Layer over a Blunt Body for Laminar, Turbulent, and Transitional Flow”, *International Journal for Numerical Methods in Fluids*, Vol. 45, March 2004, pp 1291-1351.
- ¹⁰ Walters, D.K., and Leylek, J.H., “Prediction of Boundary-Layer Transition on Turbine Airfoil Profile Losses”, ASME Paper No. IMECE 2003-41420.
- ¹¹ Walters, D.K., and Leylek, J.H., “Computational Fluid Dynamics Study of Wake-Induced Transition on a Compressor-Like Flat Plate”, *Journal of Turbomachinery*, Vol. 127, January 2005, pp 52–63.
- ¹² Sanders, D.D., O’Brien, W.F., Sondergaard, R., Polanka, M.D., and Rabe, D.C., “Predicting Separation and Transitional Flow in Turbine Blades at Low Reynolds Numbers”, ASME Paper No. GT-2008-50283.
- ¹³ Wilcox, D.C., “Turbulence Modeling for CFD”, DCW Industries, Inc., 1993.